Journal of Magnetic Resonance **138,** 288–297 (1999)
Article ID jmre.1999.1758, available online at http://www.idealibrary.com on IDEAL®

# Simulation of Magnetic Resonance Static Powder Lineshapes: A Quantitative Assessment of Spherical Codes

Alessandro Ponti[1]

*Consiglio Nazionale delle Ricerche, Centro per lo Studio sulle Relazioni tra Struttura e Reattività Chimica, via C. Golgi 19, I-20133 Milano, Italy*

Received September 29, 1998; revised February 19, 1999

**Simulation of magnetic resonance static powder spectra is performed by a (possibly weighted) summation of single-crystal spectra computed for different orientations of the external field with respect to the principal axes of the magnetic interactions. The many available methods differ in the choice of the integration points (i.e., orientations) and weights, the set of which is called spherical code. There is continuing interest in minimizing the number of integration points necessary to a good simulation. Neglecting the possible interpolation of transition frequencies and intensities between integration points, we turn our attention to the efficiency of spherical codes themselves. To this end, an unbiased quantitative procedure to assess their efficiency in simulating magnetic resonance static powder spectra is proposed. To achieve an impartial judgement, the procedure has been designed by carefully taking into consideration the following points: choice of exact reference spectra; accurate definition of the merit figures; extended range of number of integration points; orientation dependence of the efficiency. The proposed procedure has been applied to an inclusive set of 23 spherical codes. It was found that most codes perform rather similarly. SPIRAL is the most efficient code, whereas Monte Carlo and "repulsive" codes show the best rotational invariance of the simulated lineshape with respect to the orientation of the spherical code.** 

*Key Words:* **spectral simulation; static powder lineshape; spherical code.**

## INTRODUCTION

Solid-state nuclear and electronic magnetic resonance spectroscopies are powerful methods to gather information about molecular structure and dynamics. Ideally, one would study a single-crystal sample, since in such case resolution is usually sufficient to obtain the matrices of the anisotropic magnetic interactions. Unfortunately, single crystals are often difficult or impossible to prepare, but solid substances may be available as polycrystalline powder, that is, a collection of tiny crystals randomly oriented in space. Such a powder sample comprises differently oriented but otherwise identical spin systems and, therefore, a powder spectrum is the superposition of the very many spectra which, in principle, could be obtained by rotation of a single crystal. Because of the anisotropy of the magnetic interactions, spectra of powder samples are often poorly resolved. For this reason, reliable information can be extracted from powder spectra only by iterative fitting or, at least, accurate simulation.

Both simulation and fitting require computation of the lineshape for many sets of spectral parameters. Since analytic expressions for powder lineshapes are known only for a few simple cases, one must resort to numerical techniques. Up to now this problem has been tackled by the summation of single-crystal spectra computed for a number of different orientations of the external field with respect to the principal axes of the magnetic interactions. As the bottleneck of the spectral synthesis is the calculation of transition frequencies and intensities at each orientation from the eigenvalues and -vectors of the spin Hamiltonian, reducing the number of diagonalizations by carefully choosing the set of orientations (and their weights) has been a subject of continuing interest. As a result, many such sets have been proposed (*1–10*), which, following the mathematical nomenclature, we call spherical codes. There is another important method to speed up powder averaging, namely, local interpolation of transition frequencies and intensities (*1, 3, 4, 6, 8, 11*). However, to keep the paper to a reasonable length, we defer the study of interpolative methods to a future paper.

Two quantitative comparisons of spherical codes have been recently reported (*9, 10*). In the former eight spherical codes have been compared with regard to efficiency for the simulation of MAS spectra. Since it was shown that the efficiency depends on the orientation of the reference frame in which the spherical code is defined with respect to the axes of the magnetic interactions, the insensitivity of the efficiency to this relative orientation has been used as merit criterion. The new REPULSION code turned out to be the most efficient in the range of 50–250 points, relevant for the simulation of MAS spectra. In the latter study, several spherical codes have been used to compute the frequency-independent amplitude of MAS sidebands and their efficiency has been assessed. A code based on Gaussian spherical quadrature proved to be the fastest method up to about 400 points. However, a quantitative comparison of spherical codes with reference to the efficiency for

[1] E-mail address: ponti@csrsrc.mi.cnr.it.



1090-7807/99 $30.00

the simulation of *static* powder spectra is still lacking. Of course, being the simulated function different, it is possible that spherical codes rank in an order different from that in Refs. (*9, 10*). Moreover, static powder spectra may require many more orientations then MAS spectra or sideband amplitude, especially when there is large anisotropy and small homogeneous linewidth, and this can deeply affect the efficiency of spherical codes.

In conclusion, the aim of this paper is (1) to propose an unbiased quantitative procedure to assess the efficiency of spherical codes in simulating magnetic resonance static powder spectra and (2) to apply the proposed protocol to an inclusive set of spherical codes. The scope of the paper is limited to the efficiency of spherical codes in the simulation of *static* powder spectra *without* interpolation of transition frequencies and intensities. The plan of the paper is as follows: In the next section the assessment procedure is developed after a short survey of the theory of powder averaging. Then, the spherical codes are categorized and briefly described. Next, the results of extensive spectral simulations employing these codes are analyzed by the proposed procedure. Finally, the main conclusions are summarized.

## ASSESSMENT PROCEDURE

We begin this section by briefly recalling the theory of powder averaging in magnetic resonance. Consider a reference frame fixed in the laboratory (LRF) and let $\Omega$ represent the orientation of a crystallite with respect to the LRF. In general, the spectrum $s$ due to a crystallite with orientation $\Omega$ can be written as

$$s(\omega;\,\Omega) = \sum_{\text{lines}} A(\Omega)\, f[\omega - \omega_0(\Omega),\, \lambda(\Omega)], \qquad [1]$$

where $\omega$ is the frequency, $\omega_0$, $\lambda$, $A$ are the orientation-dependent position, width, and amplitude, respectively, of each line of the spectrum, and $f$ is the shape of the component lines. Assuming an isotropic distribution of the crystallites, the powder spectrum $S$ is obtained by averaging $s$ over all possible orientations of the crystallite:

$$S(\omega) = \frac{\int s(\omega;\,\Omega)\, d\Omega}{\int d\Omega}. \qquad [2]$$

In practice, one considers the equivalent problem where the crystallite is held fixed and the LRF assumes all possible orientations $\Omega$ with respect to a reference frame fixed to the crystallite (CRF). The orientation $\Omega$ is completely represented by the polar ($\theta$) and azimuthal ($\phi$) angles of $\mathbf{B}_0$ in the CRF, since the Hamiltonian is invariant under rotation about $\mathbf{B}_0$. [The anisotropic dependence of the spectral amplitude on the exciting field $\mathbf{B}_1$ is neglected since the corresponding integration can be performed analytically (*12*)]. Thus, Eq. [2] reduces to an integration over the surface of the unit sphere ($S^2$). Moreover, since the static spin Hamiltonian is invariant also for space inversion of $\mathbf{B}_0$, the integration may always be confined to a unit hemisphere:

$$S(\omega) = \frac{1}{2\pi} \int_0^{\pi/2} d\theta\, \sin\theta \int_0^{2\pi} d\phi\, s(\omega;\,\theta,\,\phi). \qquad [3]$$

Further reduction of the integration region is possible when the spin Hamiltonian possesses additional symmetry (*10*). As the double integration in Eq. [3] cannot be carried out analytically except for a few cases, one can know the integral function $S(\omega)$ only at a finite set of frequencies $\omega_m$ ($m = 1, \ldots, M$) by approximating the $M$ integrals $S(\omega_m)$ as

$$S(\omega_m) \cong \sum_{i=1}^{N} w_i\, s(\omega_m;\,\theta_i,\,\phi_i) \equiv I_N(\omega_m), \qquad [4]$$

where $N$ is the number of orientations (i.e., integration points on $S^2$) in the spherical code, and $(\theta_i,\,\phi_i)$ are the spherical coordinates of the $i$th integration point with normalized weight $w_i$. From Eq. [1] it can be seen that the integrand $s(\omega_m;\,\theta_i,\,\phi_i)$ is peaked about a narrow stripe of $S^2$ where

$$|\omega_0(\theta_i,\,\phi_i) - \omega_m| \approx \lambda(\theta_i,\,\phi_i), \qquad [5]$$

so that most of the integrand evaluations do not contribute to $I_N(\omega_m)$. For this reason, the approximate integration [4] is very demanding and standard numerical integration methods devised for smooth functions, such as Gaussian quadrature methods, are inefficient. To overcome this problem, powder averaging in the context of magnetic resonance has always been performed by a multiplex algorithm that exploits all integrand evaluations. As a preliminary step, the frequency interval of interest is divided into $M$ subintervals of constant width $\Delta$ and centered about $\omega_m$. Then, the line position and amplitude are evaluated at one orientation and the product of the line amplitude and the weight coefficient is added to the subinterval in which the computed $\omega_0$ falls. The procedure is repeated for all orientations in the chosen spherical code and finally the amplitudes accumulated in the subintervals approximate the powder lineshape. Clearly, no integrand evaluation is lost as the $M$ integrals $I_N(\omega_m)$ are calculated together. The scope of this paper is limited to this multiplex algorithm and does not include other subsidiary methods such as interpolation schemes.

In the present work, we try to keep an unbiased judgment by (1) comparing simulated spectra with exact references; (2) accurately defining the merit figures; (3) exploring a range of $N$ appropriate also for demanding simulations; (4) separately

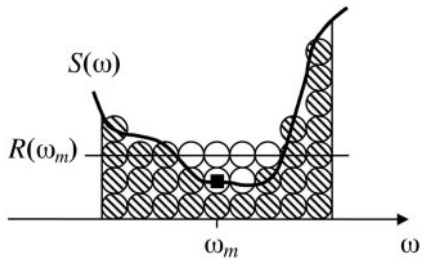


**FIG. 1.** Schematic illustration of the convergence limit of the approximate lineshape $I_N(\omega_m)$. The value of true spectrum $S(\omega)$ (thick curve) at the subinterval center $\omega_m$ is marked by a black square, whereas the average $R(\omega_m)$ of $S(\omega)$ over the subinterval is represented by a horizontal line. The hatched circles under $S(\omega)$ represent the result of the multiplex integration algorithm, i.e., the orientations at which the resonance frequency $\omega_0$ falls in the subinterval. The value $I_N(\omega_m)$ of the simulated spectrum is the number of circles divided by the subinterval width. When $N$ is large, $I_N(\omega_m)$ converges to $R(\omega_m)$ rather than to $S(\omega_m)$, as can be easily seen by reordering the circles into a rectangular array (open circles). Hence, $R(\omega_m)$ is the appropriate reference for comparison with simulated spectra.

discussing the efficiency and its orientation dependence. The procedure implementing the above points is now described in some detail. It is important that numerically integrated spectra be compared with an unbiased reference spectrum. The usual practice of using a spectrum simulated with a very large $N$ as a reference is prone to systematic error. Indeed, such a reference favors spectra simulated by the same type of code over the other ones; moreover, the latter are not correctly assessed since they are ranked by their similarity to the reference code and not to the true spectrum. To build a correct reference, one has to find an exact formula for the powder lineshape. When the spin Hamiltonian only consists of the rhombic Zeeman interaction ($\omega_1 \neq \omega_2 \neq \omega_3$), the analytical powder lineshape is available both for the secular (*13*) and for the nonsecular Hamiltonian (*14, 15*), with δ-function component lineshape. At the best of our knowledge, exact powder lineshape expressions for more complex spin Hamiltonians with rhombic symmetry have not been obtained. We therefore choose both secular and nonsecular fully rhombic spectra as reference. Full rhombicity, as opposed to the $\omega_1$–$\omega_2 \neq \omega_2$–$\omega_3$ case, and δ-function lineshape, as opposed to broader and smoother shapes, provide a more stringent test that should best discriminate between the spherical codes. Finally, it must be taken into account that, for large $N$, $I_N(\omega_m)$ does not converge to $S(\omega_m)$, but rather to the average of $S(\omega)$ over the $m$th subinterval, as pictured in Fig. 1. Accordingly, the simulated spectrum must be compared with the reference spectrum $R(\omega_m)$ obtained as

$$R(\omega_m) = \frac{1}{\Delta} \int_{\omega_m - \Delta/2}^{\omega_m + \Delta/2} S(\omega) d\omega. \qquad [6]$$

As basic figure-of-merit, we use the discrepancy $D(N)$ between the reference spectrum $R$ and the approximate spectrum $I_N$:

$$D(N) = \left\{ \frac{1}{M} \sum_{m=1}^{M} \left[ \frac{I_N(\omega_m) - R(\omega_m)}{R(\omega_m)} \right]^2 \right\}^{1/2}. \qquad [7]$$

Such $D(N)$ equally weights the error from different parts of the spectrum since it contains the sum of the squared *relative* residuals. The discrepancy has been measured for $N = 2^n$, $n = 8, 9, \ldots, 20$, that is, $256 \leq N \leq 1{,}048{,}576$, a range large enough to fully exploit the spherical codes and to cover demanding simulations such as those of large-anisotropy transition-ion EPR spectra. The efficiency of a spherical code is summarized by the convergence rate $r$ and the prefactor $p$ that are obtained by a least-squares fit to the model power-law equation

$$D(N) = pN^r. \qquad [8]$$

The efficiency of spherical codes has to be studied for different orientations $\Pi_q$ ($q = 1, \ldots, Q$) of the reference frame in which the spherical codes are constructed with respect to the CRF, where each orientation is represented by three Euler angles ($\alpha$, $\beta$, $\gamma$) (*16*). Note that the symmetry of the problem allows us to choose the $\Pi_q$ within $0 \leq \alpha, \beta, \gamma \leq \pi/2$. When there is a single dominating anisotropic interaction or when several interactions share their principal axes, we are interested in finding that $\Pi_q$ which yields the best efficiency. In this case, Eqs. [7] and [8] are sufficient to analyze the efficiency orientation by orientation. When several anisotropic interactions with noncoincident principal axes are present, each of them is differently oriented with respect to the CRF. In such a situation, one would know the average efficiency of the spherical code, and also if and to what extent spectral features due to different interactions are reproduced with unequal accuracy, because this is a source of systematic error (*9*). In order to assess the average efficiency of the code, we compute the mean discrepancy

$$\bar{D}(N) = \frac{1}{Q} \sum_{q=1}^{Q} D(N, \Pi_q), \qquad [9]$$

where $D(N, \Pi_q)$ is the discrepancy of a spherical code with orientation $\Pi_q$ and $N$ integration points, and model it to the power law in Eq. [8]. The rotational invariance may be studied by computing the relative standard deviation of the discrepancy

$$\Sigma(N) = \frac{\sigma[D(N)]}{\bar{D}(N)}$$

$$= \frac{1}{\bar{D}(N)} \sqrt{\frac{1}{Q-1} \sum_{q=1}^{Q} [D(N, \Pi_q) - \bar{D}(N)]^2}, \quad [10]$$

which measures the relative spread of the discrepancy about its mean. A global measure of the rotational invariance of the efficiency is the mean relative standard deviation

$$\bar{\Sigma} = \frac{1}{K} \sum_{k=1}^{K} \frac{\sigma[D(N_k)]}{\bar{D}(N_k)}, \quad [11]$$

where $K$ is the number of spherical codes of different size $N_k$. The efficiency of an ideal code does not depend on $\Pi$, that is, $\Sigma(N) = \bar{\Sigma} = 0$.

## SPHERICAL CODES

The efficiency of the above described multiplex integration algorithm relies on the choice of the spherical code, that is, the integration points $(\theta_i, \phi_i)$ and the weights $w_i$. All spherical codes that were found in the literature have been considered in all their variants; besides, spherical codes based on the Sobol'–Antonov–Saleev method (*17*) and codes from Refs. (*9, 10, 18*) have been applied for the first time to the simulation of powder spectra. In total, 23 codes have been studied. In this section, the spherical codes are only briefly described and the reader is referred to the literature for further detail; explicit formulas, which cannot be found in the literature, are given in the Appendix. Spherical codes can be divided into two groups: codes adapted from methods of integration on a two-dimensional planar region, and codes devised for integration on the unit sphere. We begin considering the former group.

Several planar integration methods have been applied to powder averaging by mapping the integration points from the plane onto the unit sphere by means of an inverse cartographic projection (*19, 20*). The simplest choice is the plate-carré projection that maps the $-\pi < x \leq \pi$, $0 \leq y \leq \pi$ rectangle to $S^2$ by the transformation

$$\phi = x, \quad \theta = y. \quad [12]$$

For instance, the spherical code obtained by plate-carré projection of a rectangular grid, also known as the apple-peel method (*4*), is portrayed in Fig. 2a. Each point is given an additional weight $w_i = \sin(\theta_i)$ to account for the approaching of the meridians near the poles, a fact that may degrade the performance of the underlying method. Conversely, equal-area projections do not require additional weight factors. Among these, the two most widespread are the Lambert cylindrical,

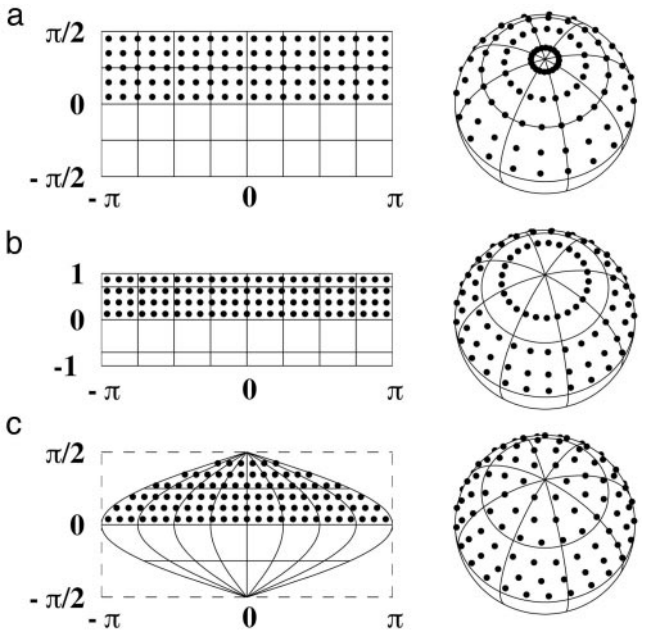


**FIG. 2.** Inverse cartographic projections used to transform integration points from a planar region (left) to the upper half of the unit sphere (right). The integration points (dots) constitute an open rectangular grid to which the usual meridian–parallel grid is superimposed. (a) Plate-carré projection; (b) Lambert cylindrical projection; (c) sinusoidal projection. The projected codes differ especially in the polar region, where points are too crowded (a), too sparse (b), and evenly distributed (c).

which transforms the $-\pi < x \leq \pi$, $-1 \leq y \leq 1$ rectangle to $S^2$ by

$$\phi = x, \quad \theta = \arccos(y), \quad [13]$$

and the sinusoidal, which maps the $-\pi \sin(y) < x \leq \pi \sin(y)$, $0 \leq y \leq \pi$ region to $S^2$ by

$$\phi = \frac{x}{\sin(y)}, \quad \theta = y. \quad [14]$$

The Lambert cylindrical projection of a rectangular grid, already known as equator centered grid (*5*) or spherical grid (*9*), accounts for the approaching meridians by taking equal steps in $\cos(\theta)$ instead of $\theta$ (see Fig. 2b). The sinusoidal projection of a rectangular grid, already known as polar centered grid (*5*) or igloo method (*8*), compensates the approaching meridians by making the number of $\phi$-steps along a parallel proportional to the length of the parallel itself, as can be seen in Fig. 2c. Many other cartographic projections are known, but a preliminary survey indicated that significant improvement over the three above projections should not be expected. Therefore, three different spherical codes (labeled PC, Cyl, and Sin) can be generated from each of the methods described in the following.

The familiar rectangular grid method (*1, 4*) consists in di-

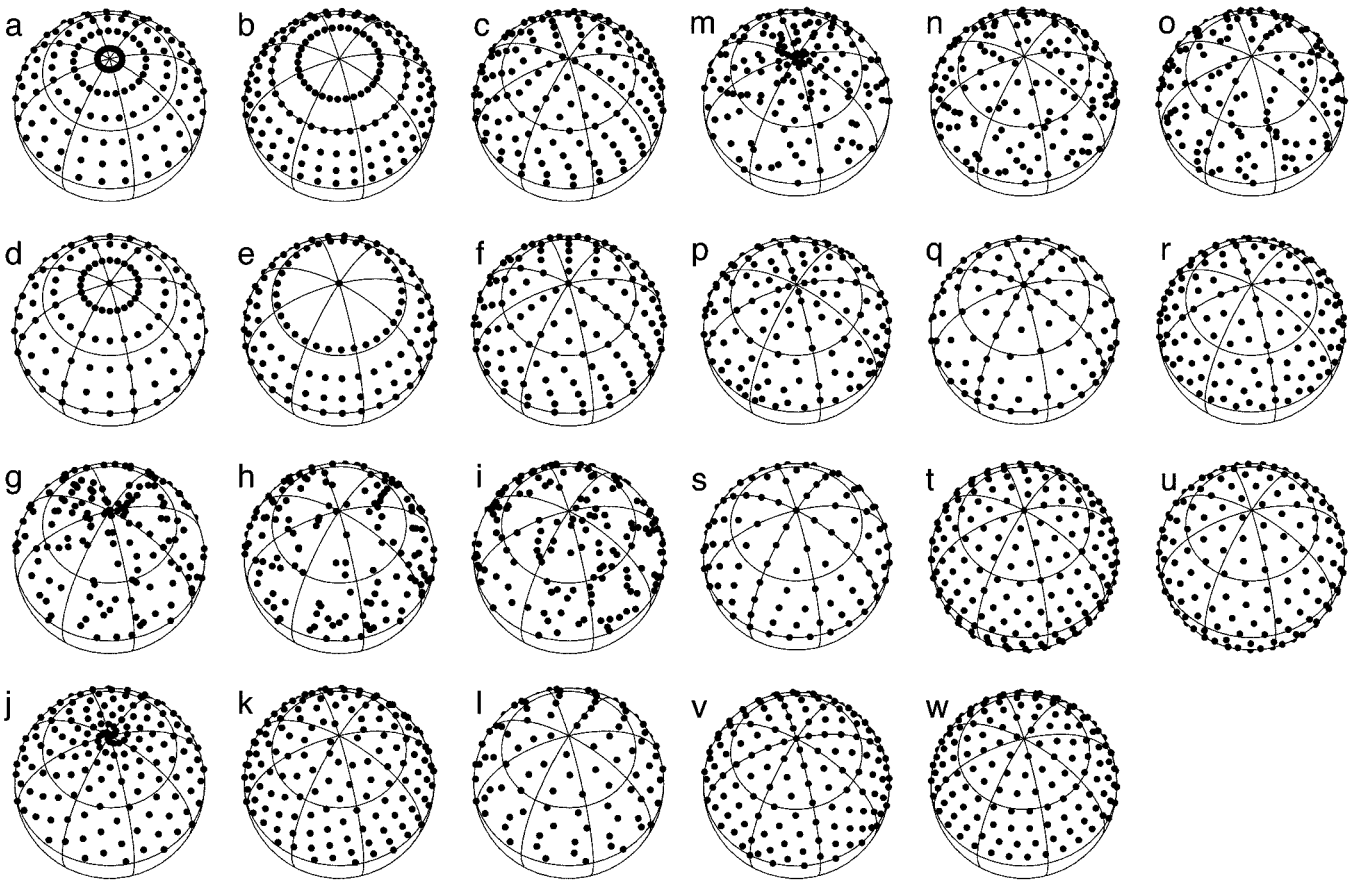


**FIG. 3.** Examples of spherical codes on the upper half of the unit sphere. For the sake of clarity, $N$ is small and the meridian–parallel grid is also visible. (a) Open PC grid ($N = 150$); (b) open Cyl grid (160); (c) open Sin grid (159); (d) closed PC grid (150); (e) closed Cyl grid (160); (f) closed Sin grid (154); (g) PC MC (160); (h) Cyl MC (160); (i) Sin MC (174); (j) PC ZCW (158); (k) Cyl ZCW (158); (l) Sin ZCW (101); (m) PC SAS (160); (n) Cyl SAS (160); (o) Sin SAS (158); (p) open ASG (144); (q) closed ASG (144); (r) open SOPHE (144); (s) closed SOPHE (144); (t) FM (289); (u) REPULSION (232); (v) LEB (151); (w) SPIRAL (160). FM and REPULSION codes are defined on the whole $S^2$ (see text).

viding the integration region into equal subrectangles. The integration points are chosen at the centers (open form, Figs. 2 and 3a–3c) or at the vertices (closed form, Fig. 3d–3f) of the subrectangles. The Monte Carlo (MC, Fig. 3g–3i) method (*2*) uses couples of uniformly distributed (pseudo)-random numbers as the coordinates of the integration points. It is important to choose a good random-number generator to avoid as much as possible correlation between the points, since this can severely affect the efficiency. In the present work a 64-bit pseudo-DES hashing generator (*17*) is used. The quasi-random methods such as that by Zaremba–Conroy–Wolfsberg (ZCW, Fig. 3j–3l) (*21–23*) optimized for anisotropic chemical-shift lineshape by Koons and co-workers (*7*), and that by Sobol'–Antonov–Saleev (SAS, Fig. 3m–3o) (*17*), here applied for the first time to powder averaging, have found widespread use in multidimensional numerical integration. The coordinates of the ZCW integration points are obtained by a global optimization, which becomes troublesome for very large $N$. In fact, the largest available set in Ref. (*7*) has $N = 16{,}574$. This disadvantage does not plague the SAS method, where coordinates are generated by closed formulas.

The second group of spherical codes comprises the "octahedral" Alderman–Solum-Grant (ASG) (*3*) and SOPHE (*8*) codes, the "repulsive" codes by Fliege and Maier (FM) (*18*) and by Bak and Nielsen (REPULSION) (*9*), the spherical Gaussian-quadrature code by Lebedev (LEB) as applied to powder averaging by Edén and Levitt (*10*), and the SPIRAL code (*6, 24*). The ASG code (Fig. 3p–3q) is obtained by first dividing each face of the octahedron inscribed in the unit sphere into equilateral triangles and then projecting the triangular mesh onto $S^2$. The code comprises either the triangle vertices (closed form) or the centroids (open form). A good approximation of the weights $w_i$ has been given. The SOPHE code (Fig. 3r–3s) is obtained by partitioning $S^2$ into triangular regions (which are not spherical triangles, however), similarly to the ASG code. Closed and open forms can be obtained as before. At the best of our knowledge, accurate weights have been computed here for the first time (see Appendix). The FM

and REPULSION codes (Fig. 3t–3u) are obtained by distributing points on $S^2$ so that a target function is minimized. The target function for FM is the sum of the inverse Euclidean distances between the points (proportional to the electrostatic potential energy), whereas for REPULSION it is the sum of the inverse geodetic distances on $S^2$ (length of great circle arcs). Both codes are usually generated on the whole $S^2$, but they can be used as such to average over one half of $S^2$ since they lack an inversion center. The LEB code with $N$ orientations (Fig. 3v) is generated by requiring that all spherical harmonics of order $L \leq L_{\max}$ be exactly integrated, where $N \cong (L_{\max} + 1)^2/3$. Therefore, an integral can be accurately computed with $N$ orientations when the integrand can be accurately expressed as a linear combination of the spherical harmonics up to and including order $L_{\max}$. The SPIRAL code (Fig. 3w) was first applied to powder averaging in Ref. (*6*), where the coordinates of the integration points were obtained by optimization. Later, these coordinates were expressed analytically in the context of magnetic resonance imaging (*24*) as follows. Consider the spherical spiral defined by the parametric equations

$$\theta = \arccos(t), \quad \phi = c \arcsin(t), \quad -1 \leq t \leq +1, \quad c \gg \pi, \quad [15]$$

where $2\pi/c$ is the spiral turn and $2c$ is the spiral length from the south to the north pole. This curve uniformly covers $S^2$ in the sense that equal $t$ intervals correspond to segments of the unit sphere with equal area. To obtain a uniform discrete sampling of $S^2$, the integration points are chosen on the spiral at a distance equal to the spiral turn. The spiral subdivision can be actually performed both in open and in closed form. However, there is no noticeable difference between them and, therefore, only the open form is considered in the following. Short C programs to generate the described spherical codes are available at http://www.csrsrc.mi.cnr.it/~ponti.

## RESULTS AND DISCUSSION

Magnetic resonance spectra have been simulated for fully rhombic Zeeman interaction, in both the secular and the nonsecular case, with $M = 100$ points on the frequency axis and $N = 2^n$ ($n = 8, 9, \ldots, 20$) orientations. Some codes, namely ZCW, FM, REPULSION, and LEB, can be found only for a narrower range of $N$. Simulations have been carried out for a set of $Q = 125$ different orientations of the SCRF with respect to the CRF consisting of a $5 \times 5 \times 5$ closed grid within the region $0 \leq \alpha, \beta, \gamma \leq \pi/2$ of the space of the Euler angles. This closed grid covers the studied $(\alpha, \beta, \gamma)$ region well in the sense that a refinement of the grid does not affect the average values. In total, 32,250 powder spectra have been computed. All computations have been performed by means of a Sun ULTRA-2 workstation.

The most general result is that there is no significant efficiency difference between the secular and the nonsecular case. This equivalence suggests that the following discussion and conclusions, rigorously valid only for powder lineshapes due to a single Zeeman interaction, have a general validity for static lineshapes. For the same reason, it suffices to report the results for the nonsecular case. A logarithmic plot of the orientation-averaged discrepancy $\bar{D}(N)$ against the number of points $N$ is shown as Fig. 4. The best-fit lines are the dotted lines in Fig. 4, and the regressed parameters $p$ and $r$ are reported in Table 1 along with the correlation coefficient $\rho$. It appears that the

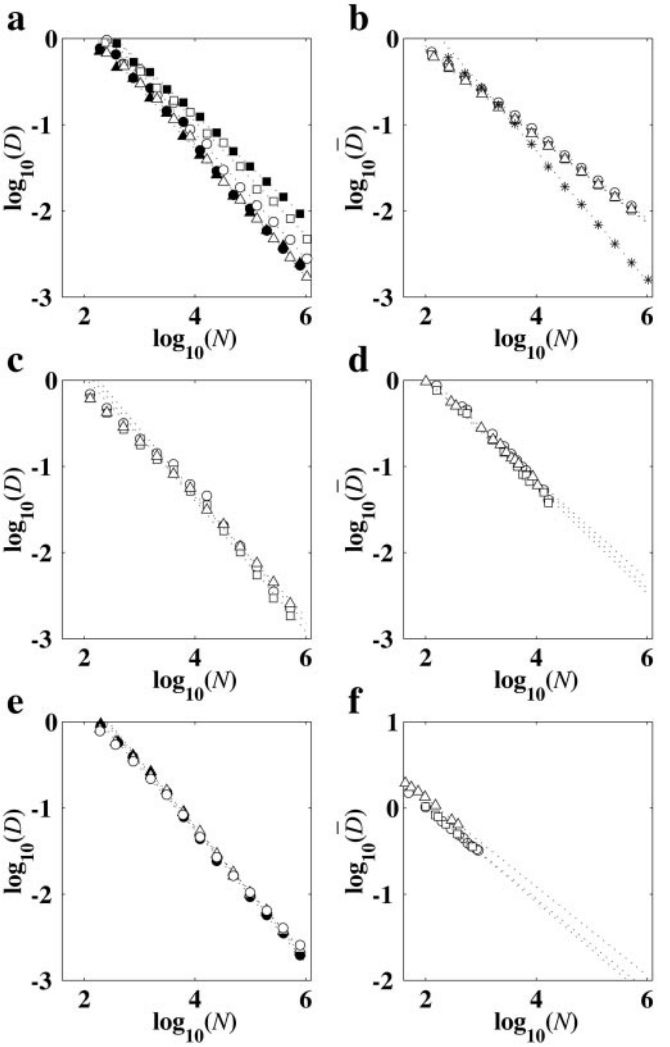


**FIG. 4.** Logarithmic plots of the mean discrepancy $\bar{D}$ against the number of points $N$. The best-fit curves appear as straight dotted lines. (a) GRID codes. Open (full) circles: open (closed) PC; open (full) squares: open (closed) Cyl; open (full) triangles: open (closed) Sin. (b) MC and SPIRAL codes. Circles: MC PC; squares: MC Cyl; triangles: MC Sin; stars: SPIRAL. (c) ZCW codes. Circles: PC; squares: Cyl; triangles: Sin. (d) SAS codes. Circles: PC; squares: Cyl; triangles: Sin. (e) ASG and SOPHE codes. Open (full) triangles: open (closed) ASG; open (full) circles: open (closed) SOPHE. (f) Circles: FM; squares: REPULSION; triangles: LEB; note the different vertical range in this panel.

**TABLE 1**
**Best-Fit Parameters $r$ and $p$ and Correlation Coefficient $\rho$ from the Least-Squares Fit of the Mean Discrepancy $\bar{D}(N)$ to Model Eq. [8]**[a]

| Spherical code | $r$ | $p$ | $\rho$ | $10^{-3}$ $N(\bar{D} = 0.01)$ | $10^{-3}$ min $[N(D = 0.01)]$ | $\bar{\Sigma}$ |
|---|---|---|---|---|---|---|
| Grid PC open | $-0.71 \pm 0.01$ | $51 \pm 7$ | $-0.9982$ | $175 \pm 50$ | 83 | $0.28 \pm 0.07$ |
| Grid Cyl open | $-0.62 \pm 0.02$ | $30 \pm 5$ | $-0.9964$ | $410 \pm 170$ | 103 | $0.40 \pm 0.10$ |
| Grid Sin open | $-0.74 \pm 0.01$ | $49 \pm 5$ | $-0.9991$ | $101 \pm 20$ | 68 | $0.20 \pm 0.05$ |
| Grid PC closed | $-0.73 \pm 0.02$ | $60 \pm 10$ | $-0.9974$ | $142 \pm 48$ | 87 | $0.25 \pm 0.06$ |
| Grid Cyl closed | $-0.59 \pm 0.01$ | $34 \pm 2$ | $-0.9994$ | $1020 \pm 180$ | 191 | $0.29 \pm 0.07$ |
| Grid Sin closed | $-0.70 \pm 0.01$ | $40 \pm 4$ | $-0.9989$ | $134 \pm 29$ | 88 | $0.21 \pm 0.05$ |
| MC PC | $-0.497 \pm 0.002$ | $11.2 \pm 0.2$ | $-0.9999$ | $1360 \pm 80$ | 992 | $0.08 \pm 0.01$ |
| MC Cyl | $-0.502 \pm 0.001$ | $10.6 \pm 0.1$ | $-0.9999$ | $1070 \pm 50$ | 772 | $0.07 \pm 0.01$ |
| MC Sin | $-0.499 \pm 0.002$ | $10.3 \pm 0.2$ | $-0.9999$ | $1090 \pm 70$ | 850 | $0.07 \pm 0.01$ |
| ZCW PC | $-0.62 \pm 0.02$ | $21 \pm 3$ | $-0.9966$ | $216 \pm 78$ | 119 | $0.16 \pm 0.08$ |
| ZCW Cyl | $-0.63 \pm 0.02$ | $19 \pm 2$ | $-0.9970$ | $175 \pm 59$ | 84 | $0.17 \pm 0.10$ |
| ZCW Sin | $-0.58 \pm 0.01$ | $14 \pm 1$ | $-0.9986$ | $294 \pm 68$ | 119 | $0.14 \pm 0.06$ |
| SAS PC | $-0.69 \pm 0.02$ | $42 \pm 10$ | $-0.9941$ | $166 \pm 85$ | 116 | $0.17 \pm 0.06$ |
| SAS Cyl | $-0.70 \pm 0.02$ | $38 \pm 8$ | $-0.9950$ | $127 \pm 60$ | 97 | $0.15 \pm 0.05$ |
| SAS Sin | $-0.66 \pm 0.01$ | $28 \pm 4$ | $-0.9981$ | $174 \pm 51$ | 119 | $0.11 \pm 0.03$ |
| ASG open | $-0.73 \pm 0.01$ | $57 \pm 6$ | $-0.9988$ | $147 \pm 34$ | 87 | $0.30 \pm 0.03$ |
| ASG closed | $-0.75 \pm 0.01$ | $71 \pm 6$ | $-0.9992$ | $141 \pm 26$ | 83 | $0.31 \pm 0.05$ |
| SOPHE open | $-0.71 \pm 0.01$ | $45 \pm 4$ | $-0.9993$ | $147 \pm 26$ | 82 | $0.28 \pm 0.02$ |
| SOPHE closed | $-0.75 \pm 0.01$ | $68 \pm 6$ | $-0.9993$ | $125 \pm 22$ | 69 | $0.25 \pm 0.03$ |
| FM | $-0.532 \pm 0.006$ | $11.8 \pm 0.4$ | $-0.9995$ | $600 \pm 100$ | 297 | $0.08 \pm 0.01$ |
| REPULSION | $-0.554 \pm 0.005$ | $13.4 \pm 0.3$ | $-0.9999$ | $441 \pm 53$ | 112 | $0.08 \pm 0.01$ |
| LEB | $-0.51 \pm 0.01$ | $13.8 \pm 0.6$ | $-0.9991$ | $1310 \pm 330$ | 172 | $0.26 \pm 0.04$ |
| SPIRAL | $-0.73 \pm 0.01$ | $41 \pm 4$ | $-0.9993$ | $83 \pm 15$ | 55 | $0.20 \pm 0.07$ |

[a] The number of points $N$ necessary to achieve a mean discrepancy $\bar{D} = 0.01$, the minimum $N$ to achieve $D = 0.01$ within the studied region, and the mean relative standard deviation $\bar{\Sigma}$ are also reported. All errors are one standard deviation (see text for their significance).

mean discrepancy can be satisfactorily represented by the power law Eq. [8] for all spherical codes. It is necessary to remark that the errors in Table 1 are largely overestimated by the least-squares method because the regression residuals are not normally distributed.[2] Therefore, the differences between the parameters are more meaningful than it may appear at first sight. The interplay of $p$ and $r$ may be confusing in the assessment of the code efficiency. Therefore, we regressed the number of points necessary to attain $\bar{D} = 0.01$, and the *minimum* number of points needed to achieve $D = 0.01$ within the studied set of orientations. The choice of 0.01 as reference discrepancy is somewhat arbitrary even if it corresponds to a satisfactory agreement between simulated and true lineshape, as shown in Fig. 5. Not to be misled by this arbitrary choice, these two quantities have been computed also for $D = 0.1$; as these do not show anything new, they are only touched upon in the following discussion. Finally, the mean relative standard deviation $\bar{\Sigma}$ of the orientation-averaged discrepancy (cf. Eq. [11]) is also reported in Table 1. The spherical codes are now analyzed in some detail.

[2] Since we do not fit experimental noisy data to the correct model but exact data to an approximate model, the residuals do not follow a normal (Gaussian) distribution. Because of the rapid fall-off of the normal distribution, points that are more-than-average displaced from the fitted curve cause a misleading overestimate of the parameter errors.

The six grid spherical codes show marked differences between themselves. The two cylindrical grids have a low efficiency mostly because of the small convergence rate, as the prefactor is rather low, while the plate-carré and sinusoidal codes have a much better efficiency. The reason for this can be traced back to the different uniformity of covering near the pole (see Figs. 2 and 3a–3f). The three Monte Carlo codes have essentially the same low convergence rate $r = -0.5$ typical of these methods, which translates in a rather poor efficiency in powder averaging, despite the very good prefactor. In fact, to achieve $\bar{D} = 0.01$, MC codes require about six times as many points as other codes (but only two times for $\bar{D} = 0.1$). The Cyl and Sin versions are almost equivalent and slightly superior to the plate-carré. The quasi-random ZCW and SAS codes show similar efficiency since the differences in $p$ and $r$ almost cancel. Unfortunately, the difficulty of computing ZCW codes makes unfeasible their extension below the threshold of $\bar{D} = 0.03$. Conversely, the SAS codes, here applied for the first time to powder averaging, can be easily computed also for very large $N$. They are slightly more efficient than the ZCW for $D \leq 0.1$. The superiority of the cylindrical variant of the ZCW and SAS codes is due, on one hand, to the weights needed for the plate-carré code, which degrade performance, and, on the other hand, to the fact that these method has been devised for

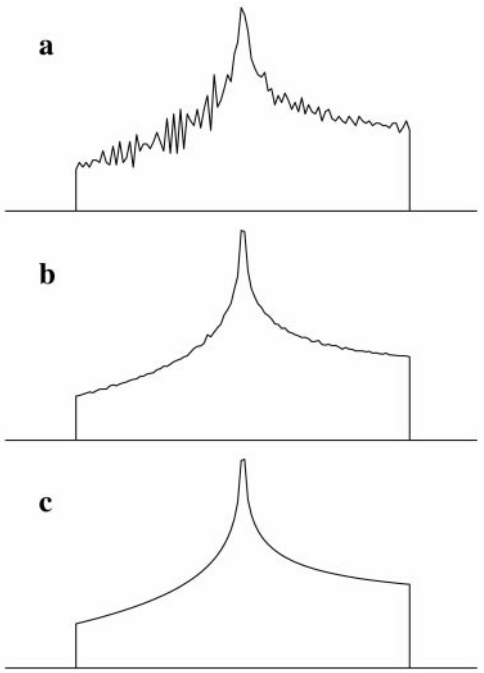


**FIG. 5.** Comparison of simulated powder lineshape for a nonsecular fully rhombic Zeeman Hamiltonian with the exact reference spectrum, pictorially showing the significance of discrepancy $D = 0.1$ and $D = 0.01$. (a) Lineshape simulated by SPIRAL code with $N = 4000$, resulting in $D = 0.1055$; (b) lineshape simulated by SPIRAL code with $N = 56{,}000$, resulting in $D = 0.0100$; (c) reference spectrum obtained by averaging the exact lineshape as in Eq. [6].

a rectangular region and not for the oval region over which the inverse sinusoidal projection is defined. The "octahedral" ASG and SOPHE codes show high convergence rates between $-0.70$ and $-0.75$. Their effect on the efficiency is, however, counteracted by the large prefactors. The slight differences in $r$ and $p$ almost vanish when we consider $N(\bar{D} = 0.01)$, which is close to 140,000 for all four codes. The "repulsive" FM and REPULSION codes and the Gaussian-quadrature LEB code show very good prefactors (12–14) but also low convergence rates close to $-0.5$. Therefore, their efficiency is rather poor and close to that of MC codes. Finally, the SPIRAL code turns out to be the most efficient. Its performance arises mainly from the high convergence rate.

The relative standard deviation $\Sigma(N)$ does not show any clear-cut trend as a function of $N$. The only discernible feature is that it grows for $N < 10^4$ and then diminishes or remains constant. Therefore, we now consider its mean $\bar{\Sigma}$ as a global measure of the rotational invariance. First, it should be remarked that the sinusoidal form always shows a better invariance than the plate-carré and cylindrical forms of spherical codes adapted from bidimensional methods. The MC, FM, and REPULSION codes show the best rotational invariance: Their efficiency can be expected to change less than 10% within the $0 \leq \alpha, \beta, \gamma \leq \pi/2$ region of the space of the Euler angles. The SAS and ZCW codes rank second with an expected change of about 15%. Sinusoidal grid and SPIRAL codes have $\bar{\Sigma} \cong 20\%$, while SOPHE, ASG, LEB, and the other grid codes can vary up to 30%. Note, however, that the poor invariance of the LEB code is due to a single outlier at the largest $N = 385$. The Cyl open grid features $\bar{\Sigma} = 40\%$. It should be noted that the codes with the best rotational invariance also have the lowest prefactors.

When there is one dominating anisotropy, the orientation $\Pi$ can be chosen at will. We therefore also looked for the orientations at which a minimum $N$ is needed to achieve $D = 0.01$ (see Table 1). Even if the efficiency range is compressed, the rank based on the minimum $N$ is the same as before. The orientation at which the minimal value is reached cannot be easily rationalized (data not shown). The spherical codes can be, however, divided in three groups. MC and SAS codes show little change within the $0 \leq \alpha, \beta, \gamma \leq \pi/2$ region; the LEB and SPIRAL codes perform best when their principal axes coincide with those of the anisotropic interaction; all other codes show their best efficiency when their principal axes do *not* coincide with those of the interaction.

Considering globally all spherical codes, the following conclusions can be drawn. (1) Monte Carlo codes have low convergence rates that yield a poor efficiency: More than $10^6$ orientations are needed to achieve a 1% discrepancy. However, they are almost independent of the relative orientation of the CRF and the SCRF. If one can afford a factor 6–10 in computation time, a possible source of error in the determination of anisotropic interaction matrices can be avoided. Note that such a factor reduces to about 2 for 10% achieved discrepancy. Recall also that the integration error can be computed only for the Monte Carlo method. (2) Planar rectangular grids projected on the unit sphere by cylindrical projection, i. e., grids with equal steps in $\cos(\theta)$ and $\phi$, have found widespread use, but they are definitely among the worst spherical codes for powder averaging. In fact, they are less efficient than all other codes (except for MC) and their efficiency is very sensitive to the relative orientation of the CRF and the SCRF. (3) The other grid codes (except for open Sin), the ZCW, SAS, ASG, and SOPHE codes perform similarly with respect to the efficiency: they require $1\text{–}3 \times 10^5$ orientations to achieve $\bar{D} = 0.01$. However, they differ in the rotational invariance, the quasi-random codes being the best ones. (4) For FM, REPULSION, and LEB we have to base our analysis on a rather limited range of $N$. Given this caveat, it can be concluded that these codes have a poor efficiency because of the low convergence rate. However, their excellent prefactor and rotational invariance (except LEB) suggest that they should be good codes for less demanding tasks, such as simulation of rotating-powder spectra, since when the needed $N$ is low the prefactor is more important than the convergence rate. The efficiency of these codes could be better than expected for $N > 1000$, but it is unlikely that they can be so extended, since it is very difficult to compute them. This is particularly true for FM and REPULSION, which are generated by a nonlinear, nonconvex con-

strained global minimization (*18*) in the presence of an exponentially growing number of local minima. It has been estimated to be about 50 for $N \cong 100$ and about 8000 for $N \cong 200$ (*25*). Such extension is certainly a formidable task. (5) Open Sin grid and SPIRAL show the highest efficiency. $\bar{D} = 0.01$ is achieved by about (or less than) $10^5$ points. In both cases, their performance arises from a high convergence rate. Unfortunately, their rotational invariance is not very good, a fact probably related to the large prefactors.

## CONCLUSIONS

A quantitative unbiased methodology to assess the efficiency of spherical codes in powder averaging of magnetic resonance spectra has been proposed. It has been applied to all published spherical codes plus new ones based on the Sobol'–Antonov–Saleev method. Equal simulation efficiency has been measured for both nonsecular and secular spectra, an equivalence suggesting that the present conclusions may have general validity. Most spherical codes (exceptions are Monte Carlo, cylindrical grid, "repulsive," and Gaussian-quadrature codes) require $1–3 \times 10^5$ integration points to achieve 1% average discrepancy ($3–6 \times 10^3$ to reach 10%). Among these, open Sin grid and SPIRAL codes stand out for their efficiency. It is striking that the simple open Sin grid code is as efficient as the SPIRAL and, even more, that it performs better than sophisticated codes. However, one should also be aware that, with the above exceptions, the studied codes differ at most by a factor of 3 in efficiency. As for the rotational invariance, the best codes are the Monte Carlo and the "repulsive." It is certainly disappointing that such codes show poor efficiency, but it should be recalled that the computational effort they require may be afforded, especially for easy simulations and/or large acceptable discrepancy.

Finally, it seems unlikely that new spherical codes can be devised that largely outperform the known ones. To obtain a large improvement in powder averaging of magnetic resonance spectra, a new approach to the problem may be more fruitful. Further investigations in this direction are presently being carried out in our laboratory (*26*).

## APPENDIX

In this appendix are collected detailed formulas that cannot be easily found in the literature about powder averaging.

### *Alderman–Solum–Grant Codes*

The following formulas refer the first octant of the unit sphere; the code on the other octants can be obtained by symmetry. $M$ is the number of subintervals on each octahedron edge. The Cartesian coordinates of the vertices of the triangular mesh on $S^2$ and the corresponding weights for the closed form of the code are

$$x_j = \frac{j}{M}, \quad j = 0, 1, \ldots, M;$$

$$y_k = \frac{k}{M}, \quad k = 0, 1, \ldots, M - j;$$

$$z_{jk} = 1 - x_j - y_k, \quad r_{jk} = \sqrt{x_j^2 + y_k^2 + z_{jk}^2}$$

$$w_{jk} = r_{jk}^{-3} \times \begin{cases} 1/6 \text{ vertex points} \\ 1/2 \text{ edge points} \\ 1 \text{ face points} \end{cases}$$

$$M = \frac{-3 + \sqrt{9 + 8(N-1)}}{2}. \quad \text{[A1]}$$

The Cartesian coordinates of the centroids of the mesh triangles on $S^2$ and the correspondent weights for the open form of the code are

$$x_j = \frac{j - 2/3}{M}, \quad j = 1, 2, \ldots, M; \quad y_k = \frac{k - 2/3}{M},$$

$$k = 1, 2, \ldots, M + 1 - j \text{ (UP triangles)}$$

$$x_j = \frac{j - 1/3}{M}, \quad j = 1, 2, \ldots, M - 1; \quad y_k = \frac{k - 1/3}{M},$$

$$k = 1, 2, \ldots, M - j \text{ (DOWN triangles)}$$

$$w_{jk} = r_{jk}^{-3}, \quad M = \sqrt{N}, \quad \text{[A2]}$$

where $z_{jk}$ and $r_{jk}$ are defined as above. In both cases, the spherical coordinates of the integration points on $S^2$ are easily obtained as

$$\theta_{jk} = \arccos(z_{jk}/r_{jk}), \quad \phi_{jk} = \arctan(y_k/x_j). \quad \text{[A3]}$$

### *SOPHE Codes*

The following formulas refer to the first octant of $S^2$; the code on the other octants can be obtained by symmetry. $M$ is the number of subintervals along $\theta$. In closed form, the integration points are the vertices of the pseudotriangular mesh,

$$\theta_j = \frac{j}{M}\frac{\pi}{2}, \quad j = 0, 1, \ldots, M; \quad \phi_k = \frac{k}{M - j}\frac{\pi}{2},$$

$$k = 0, 1, \ldots, M - j;$$

$$w_{jk} = \frac{\cos(\theta_j)}{M - j + 1} \times \begin{cases} 1/6 \text{ vertex points} \\ 1/2 \text{ edge points} \\ 1 \text{ face points} \end{cases},$$

$$M = \frac{-3 + \sqrt{9 + 8(N-1)}}{2}, \quad \text{[A4]}$$

whereas in open form they correspond to the centroids of the pseudotriangles forming the mesh:

$$\theta_{jk} = \frac{\pi}{2} \times \begin{cases} \dfrac{j - 1/3}{M} & k \text{ odd (UP pseudotriangles)} \\ \dfrac{j - 2/3}{M} & k \text{ even (DOWN pseudotriangles)} \end{cases},$$

$$\phi_{jk} = \frac{k - 1/2}{2j - 1}, \quad j = 1, 2, \ldots, M; \quad k = 1, 2, \ldots, 2j - 1$$

$$w_{jk} = \frac{\cos\left(\dfrac{j}{M}\dfrac{\pi}{2}\right)}{2j - 1}, \quad M = \sqrt{N}. \qquad \text{[A5]}$$

The weights $w_{jk}$ have been obtained by a modification of the procedure outlined in Ref. (*8*). For the open form, the weight $w_{jk}$ is the area of the pseudotriangle surrounding the centroid $jk$; for the closed form it is the pseudohexagonal region (dual of the pseudotriangle) surrounding the vertex $jk$.

*SPIRAL Code (Open Form)*

$$t_i = \frac{i - 1/2}{N}, \quad i = 1, 2, \ldots, N$$

$$\theta_i = \arccos(t_i), \quad \phi_i = \sqrt{\pi N}\,\arcsin(t_i), \quad w_i = 1. \qquad \text{[A6]}$$

An analytic expression for the weights could not be found. Therefore, a Voronoi tessellation of $S^2$ has been performed using the SPIRAL code as the set of generators. The areas of the Voronoi cells are distributed about the correct value $4\pi/N$ with standard deviation less than $(4\pi/N)/100$ for $N \geq 1000$ and a large positive kurtosis, meaning that the area distribution is much narrower than a Gaussian distribution with the same width. The assumption of unit weights is thus substantiated.

## ACKNOWLEDGMENTS

Stimulating discussions with Dr. D. Bressanini (Università dell'Insubria, Como) and Dr. M. Mella (Università di Milano) are gratefully acknowledged.

## REFERENCES


1. G. v. Veen, Simulation and Analysis of EPR Spectra of Paramagnetic Ions in Powders, *J. Magn. Reson.* **30,** 91–109 (1978).
2. S. Galindo and L. González-Tovany, Monte Carlo Simulation of EPR Spectra of Polycrystalline Samples, *J. Magn. Reson.* **44,** 250–254 (1981).
3. D. W. Alderman, M. S. Solum, and D. M. Grant, Methods for Analyzing Spectroscopic Line Shapes. NMR Solid Powder Patterns, *J. Chem. Phys.* **84,** 3717–3725 (1986).
4. M. C. M. Gribnau, J. L. C. v. Tits, and E. J. Reijerse, An Efficient General Algorithm for the Simulation of Magnetic Resonance Spectra of Orientationally Disordered Solids, *J. Magn. Reson.* **90,** 474–485 (1990).
5. A. Kreiter and J. Hüttermann, Simultaneous EPR and ENDOR Powder-Spectra Synthesis by Direct Hamiltonian Diagonalization, *J. Magn. Reson.* **93,** 12–26 (1991).
6. M. J. Mombourquette and J. A. Weil, Simulation of Magnetic Resonance Powder Spectra, *J. Magn. Reson.* **99,** 37–44 (1992).
7. J. M. Koons, E. Hughes, H. M. Cho, and P. D. Ellis, Extracting Multitensor Solid-State NMR Parameters from Lineshapes, *J. Magn. Reson. A* **114,** 12–23 (1995).
8. D. Wang and G. R. Hanson, A New Method for Simulating Randomly Oriented Powder Spectra in Magnetic Resonance: The Sydney Opera House (SOPHE) Method, *J. Magn. Reson. A* **117,** 1–8 (1995).
9. M. Bak and N. C. Nielsen, REPULSION, a Novel Approach to Efficient Powder Averaging in Solid-State NMR, *J. Magn. Reson.* **125,** 132–139 (1997).
10. M. Edén and M. H. Levitt, Computation of Orientational Averages in Solid-State NMR by Gaussian Spherical Quadrature, *J. Magn. Reson.* **132,** 220–239 (1998).
11. H. Ebert, J. Abart, and J. Voitländer, Simulation of Quadrupole Disturbed NMR Field Spectra by Using Perturbation Theory and the Triangle Integration Method, *J. Chem. Phys.* **79,** 4719–4723 (1983).
12. J. R. Pilbrow, Anisotropic Transition Probability Factor in E.S.R., *Mol. Phys.* **16,** 307–309 (1969).
13. U. Haeberlen, Ed., "High Resolution NMR in Solids," Academic Press, New York (1976).
14. F. K. Kneubühl, Line Shapes of Electron Paramagnetic Resonance Signals Produced by Powders, Glasses, and Viscous Liquids, *J. Chem. Phys.* **33,** 1074–1078 (1960).
15. V. Beltrán-López, B. Mile, and C. C. Rowlands, Exact Analytical Solution for the Powder Pattern of Orthorhombic-*g* Systems, *J. Chem. Soc., Faraday Trans.* **92,** 2303–2310 (1996).
16. H. Goldstein, "Classical Mechanics," 2nd ed., Addison-Wesley, Reading, MA (1980).
17. W. H. Press, S. A. Teukolsky, W. T. Vetterling, and B. P. Flannery, "Numerical Recipes in C, The Art of Scientific Computing," 2nd ed., Cambridge University Press, Cambridge (1995).
18. J. Fliege and U. Maier, "Charge Distribution of Points on the Sphere and Corresponding Cubature Formulae," *in* "Multivariate Approximation (Recent Trends and Results), Vol. 101, "Mathematical Research." Akademie Verlag (John Wiley Group), Berlin (1997), pp. 149–157.
19. J. P. Snyder, "Map Projections: A Working Manual," U.S. Geological Survey Prof. Paper 1395 (1987).
20. G. I. Evenden, PROJ, ver 4.3.3, 1995, available at http://kai.er.usgs.gov/ftp/PROJ.4/proj.html.
21. S. K. Zaremba, Good Lattice Points, Discrepancy, and Numerical Integration, *Ann. Mat. Pura Appl.* **4-73,** 293 (1966).
22. H. Conroy, Molecular Schrödinger Equation. VIII. A New Method for the Evaluation of Multidimensional Integrals, *J. Chem. Phys.* **47,** 5307–5318 (1967).
23. V. B. Cheng, H. H. Suzukawa, and M. Wolfsberg, Investigations of a Nonrandom Numerical Method for Multidimensional Integration, *J. Chem. Phys.* **59,** 3992–3999 (1973).
24. S. T. S. Wong and M. S. Roos, A Strategy for Sampling on a Sphere Applied to 3D Selective RF Pulse Design, *Magn. Reson. Med.* **32,** 778–784 (1994).
25. J. R. Morris, D. M. Deaven, and K. M. Ho, Genetic-Algorithm Energy Minimization for Point Charges on a Sphere, *Phys. Rev. B* **53,** R1740–1743 (1996).
26. A. Ponti, Simulation of One-Dimensional Magnetic Resonance Powder Line Shapes Reduced to Area Computation, *Chem. Phys. Lett.* **302,** 224–230 (1999).